T.-C. CHENG*, C. YU*, T.-C. YANG**, C.-Y. HUANG**, H.-C. LIN*, R.-K. SHIUE*[#]

MICROSTRUCTURE AND IMPACT TOUGHNESS OF OFFSHORE STEEL

This study focused on the effects of microstructures on the low-temperature impact toughness of directly water-quenched offshore steel. Martensite dominated the microstructure directly below the quenched surface. In contrast, mainly lower bainite, martensite, and low amount of ferrite were observed in the central region of the quenched specimen. The ductile to brittle transition temperature of tempered martensite was significantly lower than that of a bainite-dominated microstructure. It is found that low-angle boundaries within the bainite packets greatly impair the low-temperature impact toughness of the steel. The absence of high-angle boundaries in the lower bainite packets significantly deteriorates the low-temperature impact energy of offshore steel.

Keywords: low-temperature impact toughness, prior austenite grain size, hardenability, bainite

1. Introduction

Traditionally, structural alloys are developed with an eye to increasing the strength to weight ratio, reducing material costs, and reducing the energy consumed in the manufacturing process. The past few decades have seen the development of high strength low alloy (HSLA) steel, which is characterized by high strength, high toughness, and excellent weldability [1,2]. Today, this steel is widely applied in bridges, pressure vessels, and oil piping [3]. In recent years, greater attention has been focused on developing green energy to replace fossil fuel energy, and wind power capture has recently undergone rapid development [4]. As wind power harvesting has expanded, it has spread offshore, especially in the North Sea, where floating turbine foundations made of HSLA steel can weigh as much as 200 tons [3]. However, the progress in developing offshore-grade HSLA steel is still behind that of land-based HSLA steel. To apply HSLA steel in various offshore applications, it is crucial to develop high-performance HSLA steel [5]. Such steel will be suitable not only for offshore wind power applications, but also for offshore infrastructure, such as jacket structures and mobile jack-ups.

In developing the next generation of steel for offshore application, researchers propose combining the thermo-mechanical controlled process (TMCP) with online direct quenching (DQ) as a green process [6]. Before being adopted for offshore application, however, the performance of HSLA steel produced by the TMCP+DQ process needs to be evaluated. In thick steel plate, namely, that having a thickness of greater than 30 mm, the microstructures of the surface and central regions are quite different due to the insufficient hardenability of HSLA steel. This is an important consideration for HSLA steel, because its mechanical properties, and especially to the low-temperature toughness, which is a major concern in offshore applications are strongly related to the microstructure. In fact, the low-temperature toughness requirement of offshore steel is much stricter than that of most land-based structural steel. Therefore, the purpose of this research was to examine the microstructure and low-temperature toughness of HSLA steel for offshore application, and thereby to determine the key parameters affecting the low-temperature impact toughness of offshore steel.

2. Material and methods

The steel was designed according to the Norsok M-120 MDS Y70 standard [5,7]. The chemical composition of the offshore steel examined in this study was, in wt.%, 0.104 C, 0.186 Si, 0.889 Mn, 0.012 P, 0.001 S, 0.806 Ni, 0.393 Cr, 0.001 Nb, 0.016 Ti, 0.261 Mo, 0.199 Cu, 0.004 V, 0.001 B, and the balance Fe. The steel billet was hot rolled from 130 mm to a thickness of 50 mm, and then directly water-quenched from 1173 K to room temperature. The dimensions of the resultant DQ steel plate were 200 mm in width, 1,000 mm in length, and 50 mm in thickness. The specimens for metallographic examination and Charpy impact tests were machined perpendicularly to the rolling direction (RD). Charpy impact test specimens were machined from the steel plate along the transverse direction (TD). Specimens cut from the surface (S) and central (C) regions of the DQ steel plate were respectively designated as DQ-S and DQ-C. The surface and central regions of the DQ specimen were respectively de-

* NATIONAL TAIWAN UNIVERSITY, DEPARTMENT OF MATERIALS SCIENCE AND ENGINEERING, TAIPEI 106, TAIWAN
** CHINA STEEL CORPORATION, HSIAO KANG, KAOHSIUNG 812, TAIWAN
# Corresponding author: rkshiue@ntu.edu.tw

fined as 0-10 mm and 20-30 mm below the quenched surface. Specimens machined from the surface and central regions of the DQ steel and tempered at 853 K for 1800 s were designated as DQT-S and DQT-C, respectively.

An additional concern in offshore steel is its weldability. Due to the insufficient hardenability of the steel, bainite tends to develop in the heat affected zone (HAZ) of thick plate welds. In addition to being quenched and tempered, the steel used in this study was also austempered to evaluate the effects of bainite formation on the low-temperature toughness. According to JMatPro database, the simulated Ms temperature is 685 K [3,5]. The steel was austenitized at 1,173 K for 300 s and subsequently quenched in a 703 K salt bath for 1,800 s.

Vickers microhardness tests of the steel after direct water quenching and subsequent tempering were performed using an Akashi MVK-E tester with a load of 500 g for a duration of 15 s. Charpy impact tests were performed according to the ASTM A370-07a specification. Metallographic specimens were etched with 2 vol.% nital for general purpose optical microscope observation. Selected specimens were etched with picric acid for inspection of the prior austenite grain (PAG) size with optical microscopy. Microstructural analyses of specimens were performed using a scanning electron microscope (SEM, FEI NOVA 450) and a transmission electron microscope (TEM, FEI Tecnai

G2 F20). All EBSD and TEM specimens were prepared with a twin-jet polisher. The solution used in the twin-jet polisher was comprised of 85 vol.% ethyl alcohol, 10 vol.% perchloric acid, and 5 vol.% glycerol. The twin jet polisher was operated at 30 V and 243 K. An EBSD installed in the SEM was applied for crystallographic analysis, and TEM was used to identify various structures in the DQ-C specimen.

3. Results and discussion

3.1. Microstructures and microhardness depth profiles

Fig. 1 shows metallographic analysis results of the DQ-S specimen. Lath martensite dominated the surface region of the specimen, as displayed in the nital etched image of Fig. 1a. Fig. 1b presents the picric acid etched image, which reveals the prior austenite grain (PAG) morphology. The PAGs presented the classic pancake structure, with lengths of 50-150 μm along the major axis and 20-50 μm along the minor axis. Additionally, partial dynamic recrystallized PAGs can be observed among the pancaked PAGs.

Fig. 2 displays metallographic images of the DQ-C specimen. The microstructure of this specimen was very different
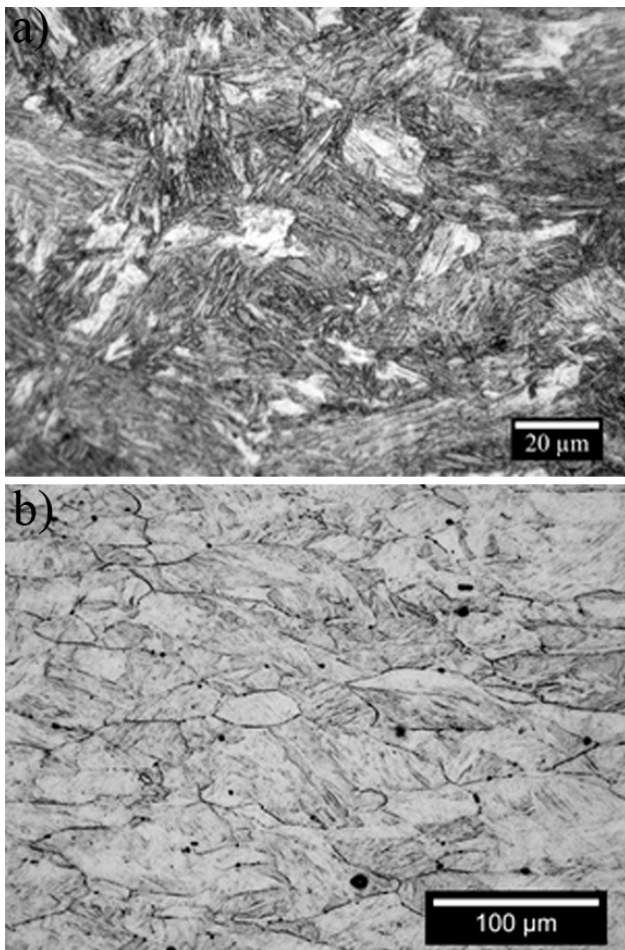

Fig. 1. Optical microstructure of the DQ-S specimen: (a) general microstructure; (b) prior austenite grains
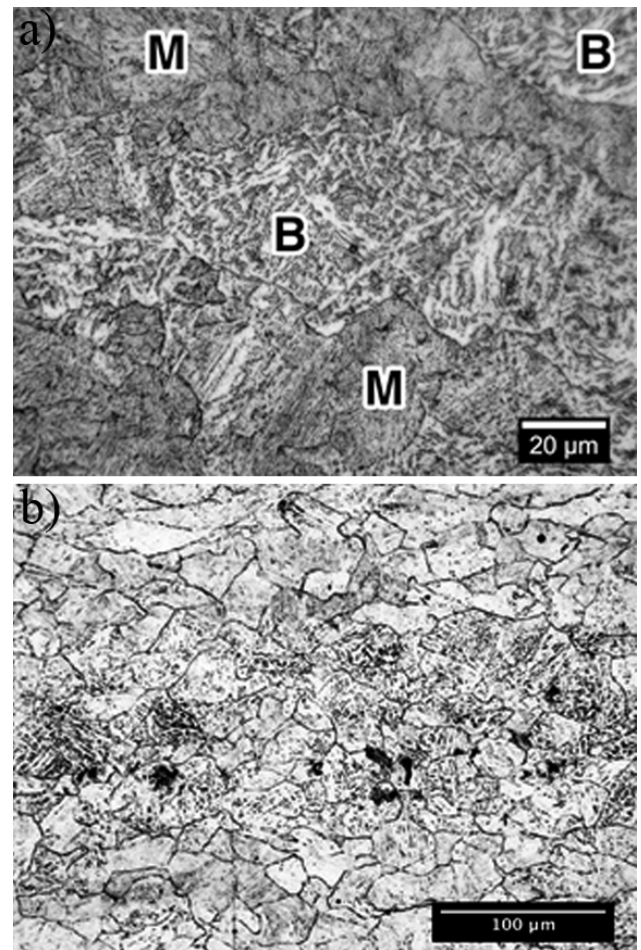

Fig. 2. Optical microstructure of the DQ-C specimen: (a) general microstructure; (b) prior austenite grains (M: martensite; B: bainite)

from that of the DQ-S one. The banded mixture of martensite and bainite is clearly visible (Fig. 2a). The combination of martensite and bainite varies with the depth below the quenched surface. In the central region of the DQ specimen, martensite comprised less than 50 vol.% of the region, and its microstructure was dominated by bainite due to the insufficient hardenability of the steel and slower cooling rate. Fig. 3 presents TEM bright field images of the DQ-C specimen in detail. Fig. 3a displays lath martensite, marked by M in Fig. 2a, and the bainite in that figure, marked by B, is lower bainite. Therefore, the microstructure of the DQ-C specimen was primarily comprised of lower bainite (B) and lath martensite (M), as illustrated in Fig. 2a.
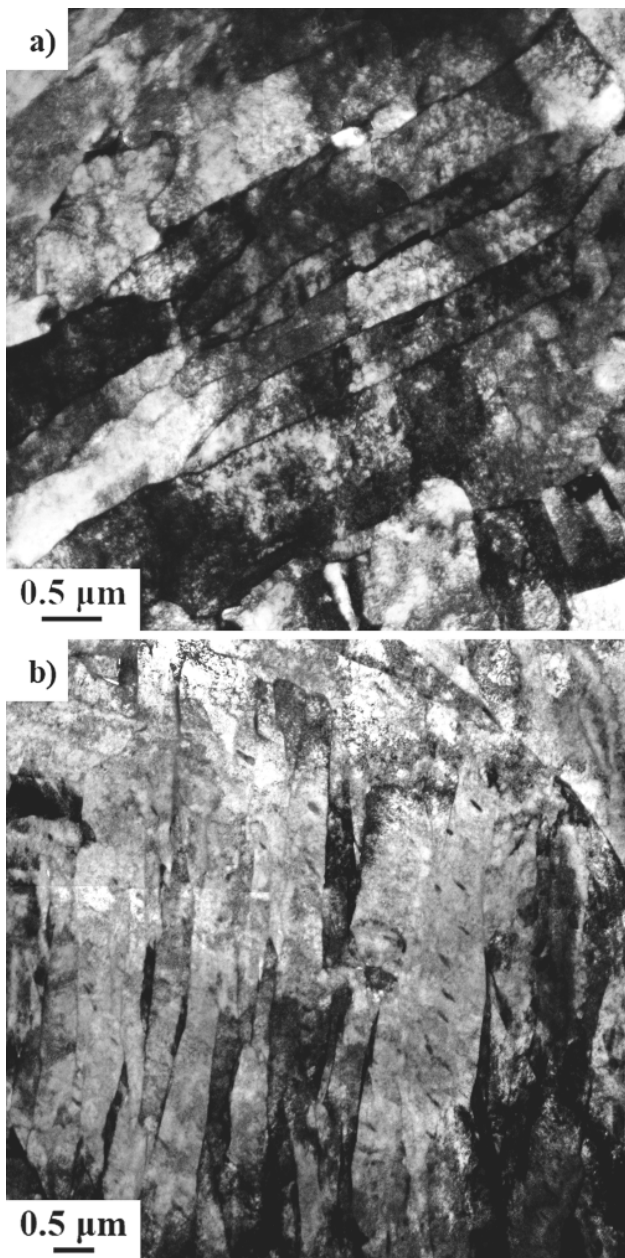

Fig. 3. TEM bright field images of the DQ-C specimen: (a) lath martensite; (b) lower bainite

Fig. 2b illustrates the morphology of PAGs in the DQ-C specimen, which was very different from that in the DQ-S one

(Fig. 1b). Equi-axed PAGs with sizes of 20 to 50 μm dominated the entire central region of the specimen, and only a few pancaked PAGs were found in the central region of the specimen. The average PAG size in the central region was approximately 30 μm. The lower bainite formed due to the insufficient hardenability of the DQ-C specimen. The hardenability of steel is strongly related to the grain size of PAGs before direct water quenching of hot rolled HSLA steel.

Fig. 4 illustrates the microstructural evolution of the water quenched steel below the quenched surface, with various PAG sizes simulated by JMatPro database [3,5]. It is obvious that the hardenability of steel increased with increasing PAG size. According to the simulation results, the entire DQ-S specimen, up to 10 mm below the quenched surface, had sufficient hardenability, resulting in the formation of martensite-dominated microstructure. The change in PAG size had little effect on the formation of martensite. The microstructure of the DQ-S specimen contained over 90 vol.% martensite, even for the PAG size smaller than 20 μm. In contrast, the PAG size significantly affected the microstructure of the DQ-C specimen. In Fig. 4, the ratio between bainite and martensite at a depth of 25 mm below the quenched surface changed from 8:1 for the 20 μm PAG size to 2:8 for the 50 μm PAG size. Based on Fig. 4, it appears that the microstructure of the DQ-C specimen was comprised of approximately 48 vol.% bainite, 47 vol.% martensite and 5 vol.% ferrite. The JMatPro simulated result was consistent with experimental observation.
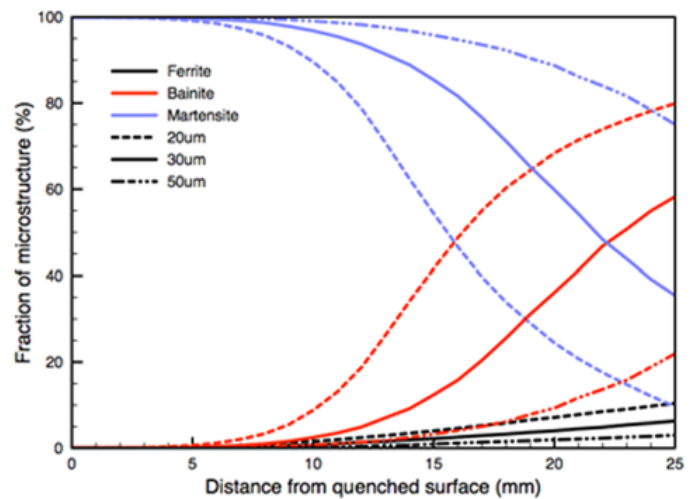

Fig. 4. Fractions of different microstructural components below the quenched surface simulated by JMatPro with various prior austenite grain sizes

Fig. 5 shows the Vickers microhardness profiles of DQ and DQT specimens. For the DQ specimen, the surface hardness was as high as 380 HV, and the lowest hardness in the central region of that specimen was 250 HV. The measured microhardness data varied greatly in the central region of the DQ specimen due to the presence of multiple structures. The hardness decreased significantly from the surface to the central region of the DQT specimen. The maximum hardness of the DQT specimen was 308 HV, and its lowest hardness was 240 HV as illustrated in the figure.
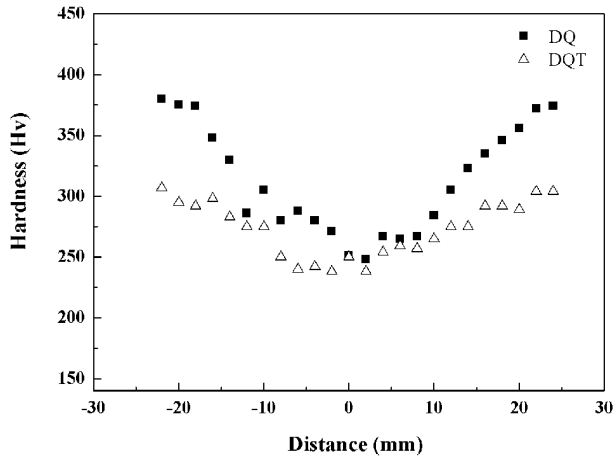
Fig. 5. Vickers microhardness profiles of the DQ and DQT specimens

3.2. Charpy impact toughness at various temperatures

Figure 6 shows the Charpy impact energy curves of DQT-S and DQT-C specimens under various testing temperatures ranging from 193 K to room temperature (300 K). The impact energies of both specimens tested at room temperature were excellent, exceeding 230 J. The average impact energy of the DQT-C specimen, 265 J, was slightly higher than that of the DQT-S specimen, 238 J. For the DQT-S specimen, the impact energy did not decrease until the testing temperature fell below 213 K. In contrast, the impact energy of DQT-C specimen quickly declined from 265 J at room temperature to 12 J at 223 K. The toughness in the center was always lower than that near the surface due to segregation and inclusions. Since the steel billet was hot rolled from 130 mm into 50 mm in thickness, and the average reduction in thickness of the plate was approximately 60%, it is reasonable that the segregation in the center of the plate was more prominent than that at the surface and resulted in the lower impact energy of the DQT-C specimen.
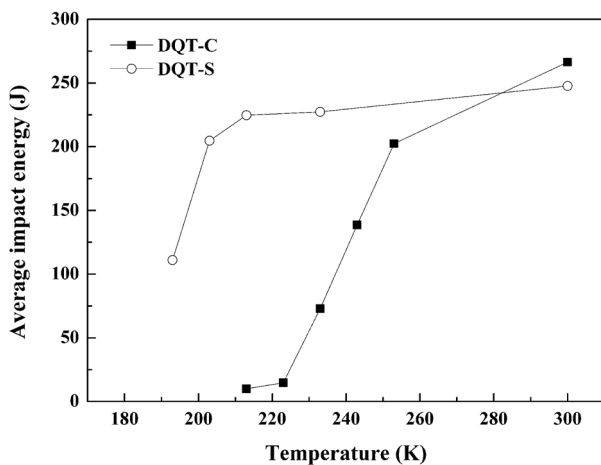

Fig. 6. Temperature-dependent Charpy impact energy curves of DQT-S and DQT-C specimens

Many factors, such as crystal structure, chemical composition, grain size and microstructure, affect the ductile to brittle

transition temperature (DBTT) curves. The BCC structure transitions from ductile to brittle is due to the limited active slip systems operating at low temperature [8]. The C and Mn contents in steel have been observed to change the DBTT behavior, and Mo and Nb can raise the DBTT of the steel if a coarse martensite-austenite structure is formed [9]. Experimental results have indicated that larger grain sizes increase the DBTT of martensitic and bainitic steels and narrow the range of the service temperature [10,11]. The DBTT of martensite can be improved by tempering and produce a better combination of strength and impact toughness. This is consistent with the current results.

It is noted that the ductile to brittle transition temperature (DBTT) of the DQT-S specimen was much lower than that of the DQT-C one. The toughness of the DQT-S sample was much higher than that of DQT-C sample below 253 K. The DBTT of steel is strongly related to its microstructure, and the microstructure of the DQT-S specimen was mainly dominated by tempered martensite. In Fig. 6, there is only one smooth ductile-brittle transition curve, which dropped at 213 K for the DQT-S specimen. On the other hand, the DQT-C specimen was comprised of approximately 50 vol.% lower bainite, tempered martensite, and some amount of ferrite as illustrated in Fig. 2a, Fig. 3, and Fig. 4. The impact energy of the DQT-C specimen significantly decreased at 233 K. It is inferred from these results that the DBTT of the bainite was much higher than that of the tempered martensite. Similar results have been reported in studies of linepipe steels [12,13].

In order to confirm that the deterioration in impact toughness (or higher DBTT) was primarily caused by the presence of lower bainite, Charpy impact tests of the austempered specimen were performed at 233 K. The austempered sample was designed to obtain a bainite-dominated microstructure. The impact energy at 233 K of the austempered specimen was 10 J. In other words, at 233 K, the impact toughness of the austempered specimen dominated by bainite was significantly lower than that of tempered martensite, 240 J.

3.3. Crystallographic analysis

One of the mechanisms proposed to explain the impact toughness deterioration of the bainitic structure is related to the presence of low-angle boundaries within the bainite packets [13]. Fig. 7 shows the EBSD crystallographic analysis results of the DQT-S specimen. Fig. 7a is the inverse pole figure (IPF) of tempered martensite. The misorientations of the tempered martensite lath boundaries were distributed quite differently in the surface region of the specimen. High-angle boundaries, i.e., misorientation > 15°, dominated most of the areas in this region, indicated by blue lines in Fig. 7b. According to the EBSD analysis results, the ratio between high-angle and low-angle (misorientation < 15°) boundaries was 70:30.

The DQT-C specimen contained two types of misorientation in martensite and bainite packets, as displayed Fig. 8. One was contributed by tempered martensite in isolated packets with high-angle boundaries, similar to that of the DQT-S specimen,
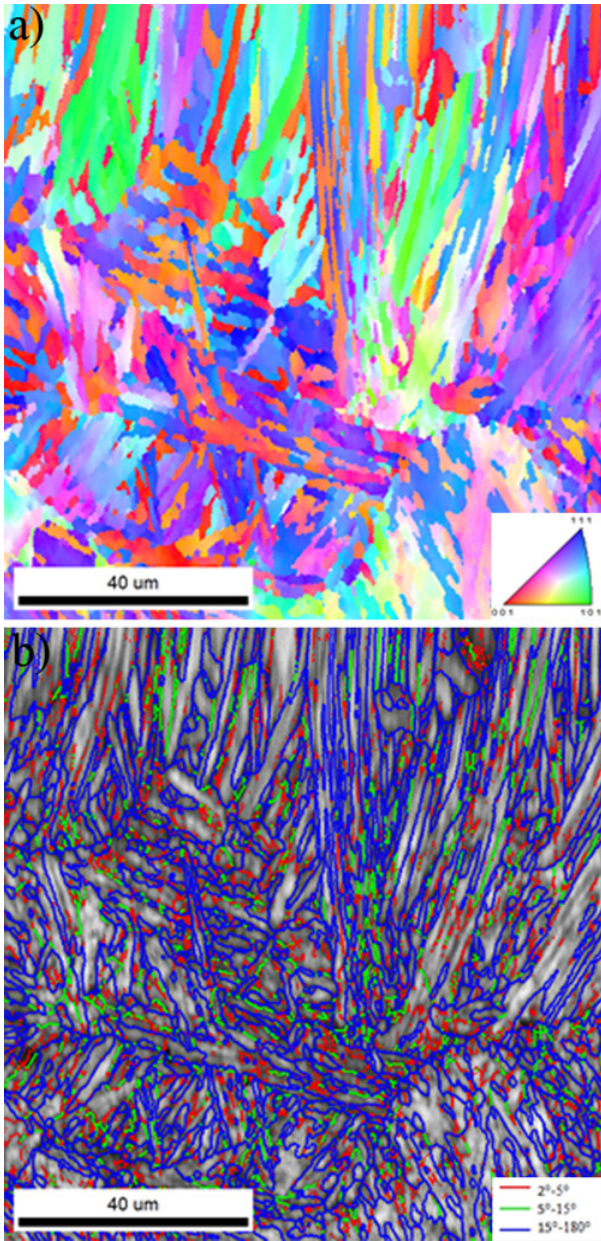
Fig. 7. EBSD analysis results for DQT-S specimen: (a) IPF; (b) boundary misorientation

Fig. 8. EBSD analysis results for DQT-C specimen: (a) IPF; (b) boundary misorientation (M: martensite; B: bainite)

as shown in the blue area (marked by M) of Fig. 8b. The other resulted from bainite packets with low-angle boundaries as illustrated by red and green areas (marked by B) in Fig. 8b. The ratio of high-angle to low-angle boundaries for the DQT-C specimen was 42:58, which was much lower than that for DQT-S one (70:30). Although high-angle boundaries were observed between the martensite and the bainite packets, low-angle boundaries were widely observed within the bainite packets. The absence of high-angle boundaries in the bainite packets significantly degraded the low-temperature impact toughness of the DQT-C specimen.

EBSD crystallographic analyses of the austempered specimen were also conducted in the experiment, and the results are shown in Fig. 9. The boundaries of bainite packets in Fig. 9a are highlighted in black for the reader's convenience. The microstructure of the austempered specimen was dominated by bainite. A similar color is obvious in the single bainite packet, as displayed in
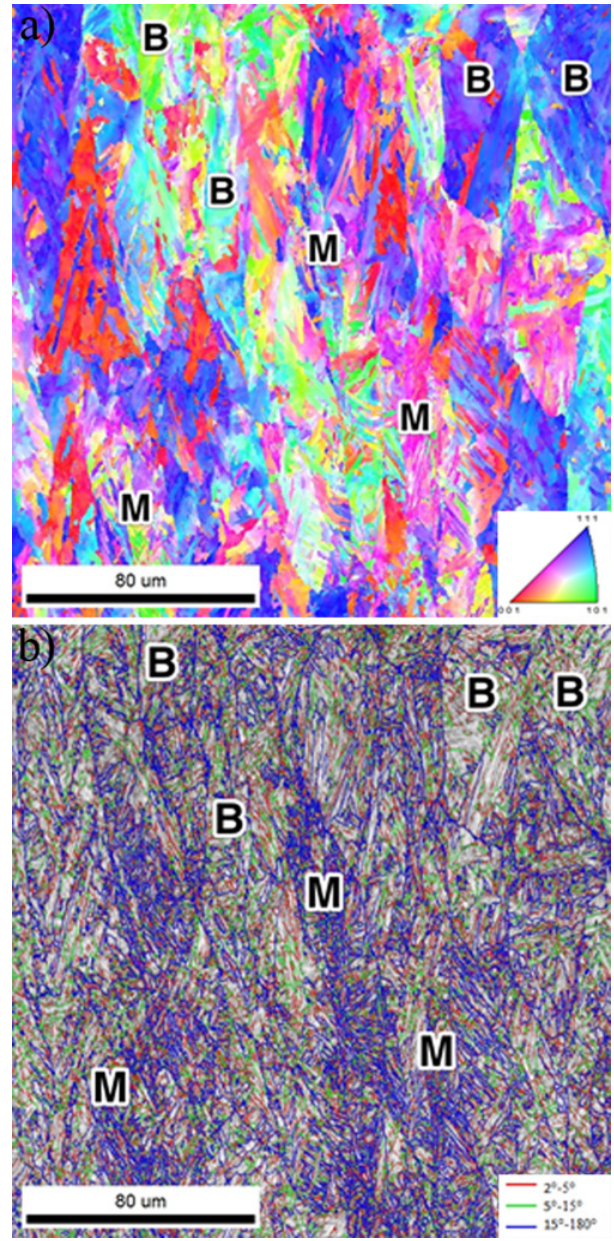
the IPF of Fig. 9a. This similarity indicates that the misorientation of boundaries within the bainite packet was quite low. Actually, the misorientation within the single bainite packet was much lower than 15°, as illustrated in Fig. 9b. Some boundaries misorientations within the bainite packet were too low (< 2°) to be identified by EBSD analyses; these are represented by the gray areas in Fig. 9b. The ratio of high-angle to low-angle boundaries was 36:64, which is even lower than that of the DQT-C specimen (42:58). The low-angle boundaries within bainite packets are detrimental to the low-temperature toughness of steel and thus should be minimized for industrial applications. For example, bainite may form in the heat affected zone of welds in structural applications [14,15]. Therefore, great caution should be paid in controlling the welding in order to prevent the formation of bainite. It has been reported that alloying with rare earth metals can modify the low-temperature toughness of the G17CrMo5-5 cast steel,

and such modification provides a good approach for engineering applications [16]. The application of EBSD combined with SEM demonstrates an effective approach for analyzing the misorientation angles of boundaries between bainite laths in packets. This approach can be applied in industry to rapidly evaluate the suitability of the steel and/or its welds for use at low-temperatures.

4. Summary

The effects of microstructures on the low-temperature impact toughness of directly water-quenched steel has been evaluated. The DBTT of a tempered martensite-dominated microstructure is significantly lower than that of a lower bainite-dominated microstructure. The low-temperature (233 K) impact energy of the martensite-dominated structure is 238 J, which is much higher than that of the lower bainite-dominated structure, 70 J. Furthermore, the impact energy of an austempered specimen tested at 233 K was as low as 10 J. It is found that the existence of low-angle boundaries within the bainite packets of lower bainite greatly deteriorates the low-temperature impact toughness of the steel. The ratio of high-angle (>15°) to low-angle (<15°) boundaries in the central region dominated by bainite is 42:58, which is much lower than that of the surface region dominated by martensite (70:30). Although high-angle boundaries were observed between martensite and lower bainite packets, low-angle boundaries were widely observed within lower bainite packets.
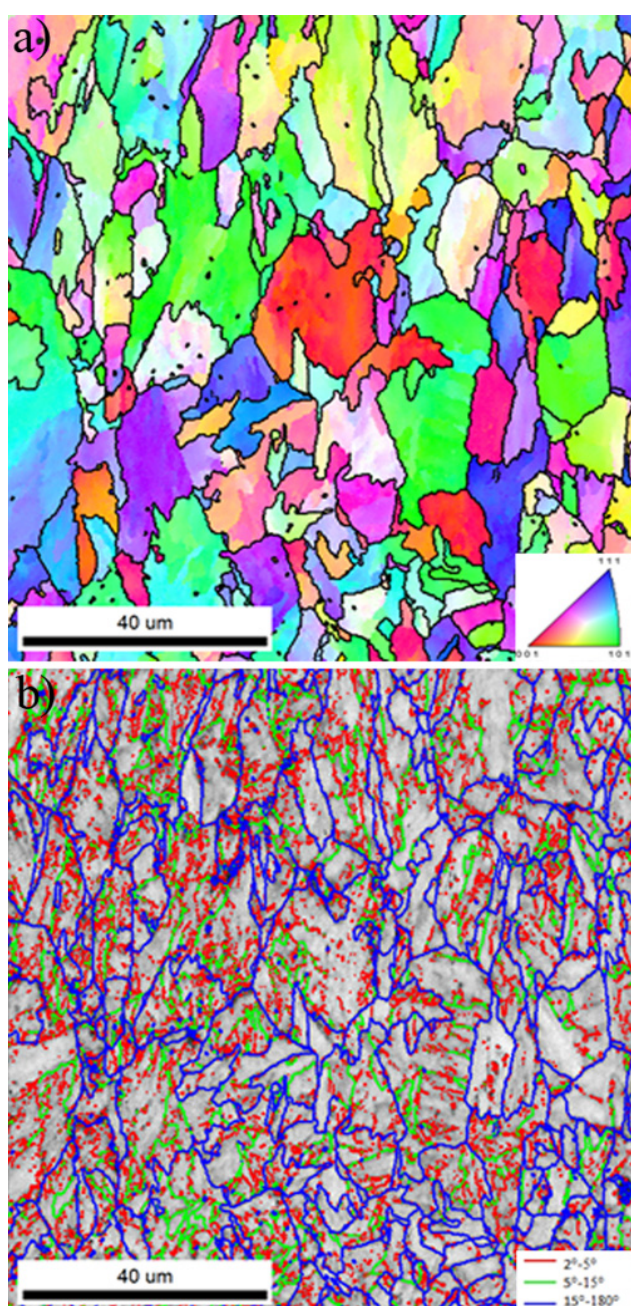
Fig. 9. EBSD analysis results for 703 K austempered specimen: (a) IPF; (b) boundary misorientation

REFERENCES

[1] G. Tither, Z. Shouhua (Eds.), HSLA Steels, Processing, Properties and Applications, 1992 The Minerals, Metals & Materials Society, Warrendale.

[2] T. Gladman, The Physical Metallurgy of Microalloyed Steels, 1997 Institute of Metals, London.

[3] T.C. Yang, C.Y. Huang, T.C. Cheng, C. Yu, R.K. Shiue, Adv. Mater. Res. **936**, 1312-1316 (2014).

[4] M. Kapsali, J.K. Kaldellis, Offshore Wind Power Basics, 2012 Technological Education Institute of Piraeus, Athens.

[5] T.C. Cheng, C. Yu, T.C. Yang, C.Y. Huang, H.C. Lin, R.K. Shiue, Mater. Res. Innov. **19** (Suppl. 9), 69-72 (2015).

[6] G. Heigl, H. Lengauer, P. Hodnik, Steel Res. Intl. **79** (12), 931-937 (2008).

[7] Norsok Standard, Material Data Sheets for Structural Steel, Rev. 3, 2000, Norway Technology Center, Oslo, Norway.

[8] T. Hanamura, F. Yin, K. Nagai, ISIJ Inter. **44** (3), 610-617 (2004).

[9] N. Isasti, D. Jorge-Badiola, M.L. Taheri, P. Uranga, Metall. Mater. Trans. **45A**, 4972-4982 (2014).

[10] A.L. Wojcieszynski, W.M. Garrison, A.W. Thompson, Scripta Metall. Mater. **27,** 851-854 (1992).

[11] H. Halfa, J. Mine. Mater. Charac. Eng. **2**, 428-469 (2014).

[12] Y.M. Kim, S.K. Kim, Y. J. Lim, N.J. Kim, ISIJ Inter. **42**, 1571-1577 (2002).

[13] X. Wu, H. Lee, Y.M. Kim, N.J. Kim, J. Mater. Sci. Technol. **28**, 889-894 (2012).

[14] P. Brziak, M. Lomozik, R. Mizuno, F. Matsuda, Archiv. Metall. Mater. **56** (2), 205-216 (2011).

[15] H.Q Yan, K.M. Wu, H.M. Wang, L. Li, Y.Q. Yin, N.C. Wu, Sci. Tech. Weld. Joi. **19** (4), 355-360 (2014).

[16] I. Dzioba, I. Kasinska, R. Pala, Archiv. Metall. Mater. **60** (2), 773-777 (2015).